Shape relaxation of gelling droplets

Julie Godefroid, Alba Marcellan, David Bouttes, Etienne Barthel, Cecile Monteux

Surface stress and shape relaxation of gelling droplets

J. Godefroid [1,2], D. Bouttes [2], A. Marcellan [1], E. Barthel [1], C. Monteux [1]

september 2023

[1] Soft Matter Science and Engineering, ESPCI Paris, PSL Research University, CNRS, Sorbonne Universités, 75005 Paris, France

[2] Saint-Gobain Research Provence, Cavaillon, France

1 Abstract

Solidification is a heterogeneous transformation from liquid-to-solid which usually combines transport, phase transition and mechanical strain: predicting the shapes resulting from such a complex problem is fascinating and has a wide range of implications from morphogenesis in biological tissues to industrial processes. For soft solids initially at equilibrium, elastic stresses, whether tensile or compressive, can be induced by heterogeneous volumetric deformations of the material and trigger instabilities and shape changes. In this article we study the shape evolution of elongated droplets of polymer

and particles suspensions undergoing a solidification process caused by the inward diffusion of a gelling agent from the surface. We show experimentally and numerically that there appears a layer of gelled material growing at the surface. Due to volume contraction, this layer induces tensile stresses and drives a flow in the ungelled liquid core, resulting in the relaxation of the droplets toward spherical shapes. Over time the thickness of this elastic membrane grows hence the bending stiffness required to change its shape eventually balances the surface stresses, which arrests the relaxation process. These results provide general rules to understand the shape of solidifying materials combining both tension and bending driven deformations.

2 Introduction

Droplet solidification is an out of equilibrium process encountered in many practical situations such as encapsulation [1], freeze casting [2] or inkjet printing [3] that can be triggered by solvent evaporation, a chemical reaction or temperature variation. Yet predicting the final shape of solidifying structures is difficult because of the multiple phenomena involved including surface energy, mass, momentum and heat transport, phase changes and mechanical deformation [4, 5, 6, 7]. From a numerical and experimental point of view the difficulty arises from the fact that mass and momentum transport, controlled respectively by diffusivity and viscosity, usually occur over different times scales hence sophisticated numerical or experimental techniques are required to obtain a full picture of the processes at play [8]. In this article we focus on the shape control of droplets of suspensions composed of a charged

biopolymer – alginate – and inorganic particles in water as they undergo a physical gelation. The solidification is triggered by the diffusion of a divalent ion – calcium – through the droplets that binds the polymer chains together to form hydrogel beads. Due to the bridging of the polymer chains by the divalent ion, a phase separation is observed [9, 10, 11, 12], called syneresis, in which the polymer chains form a dense hydrogel phase while a large fraction of the water is expelled out of the hydrogel.

For hydrogels initially at equilibrium, solvent absorption or rejection can trigger tensile and compressive stresses leading to curvature variations [12]. A typical example is the bimorph in which a volume variation of a hydrogel attached to a thin and elastic substrate results in a compressive stress if the hydrogel is swelling [13, 14, 15, 16] or a tensile stress for a negative volume contraction [17]. Both stresses result in a curvature variation. Even more complex variations of shape and curvature [18] can be obtained using various instabilities [19] such as creasing [20], wrinkling [13] or buckling based mechanisms [17, 18]. One can also observe a curvature variation by inducing a gradient in cross linking density across the material [14, 16, 21].

In the above examples curvature control was obtained for soft and thin solids initially at equilibrium. In this article we show that curvature control can be achieved in an out of equilibrium situation where droplets turn into a solid by a gelation reaction that triggers water expulsion. We use a simple experimental system. Aqueous droplets containing a polymer as well as particles are dripped into a water bath containing a gelling agent: as it diffuses into the droplets, they are turned into a solid. However, upon impact with the bath, the droplets elongate as their kinetic energy is transformed

into interfacial energy. Once they reach the bottom of the bath, we observe their shape evolution during the gelation process. Over time the elongated gelling droplets relax toward a spherical shape. We also evidence a volume contraction causing water expulsion from the growing gelled layer. We suggest that this volume contraction induces tensile stresses in the gelled layer and drives the relaxation of the elongated droplets toward spherical shapes. However in some situations this relaxation process remains incomplete. To better understand the mechanisms driving the relaxation or its arrest, we also performed numerical simulations to indentify the minimal ingredients that enable to reproduce qualitatively the experimental observations. Our simulations take into account the diffusion of ions into the droplets and the subsequent solidification near the surface as well as the volume contraction of these gelled layers.

Our results show that tensile stresses in this gelled membrane induce pressure gradients in the ungelled liquid core and drives a viscous flow from the highly curved regions to the less curved regions wherefrom shape relaxation ensues. A systematic exploration of the physical parameter space reproduces well the experimental phenomenology. Finally, for a more explicit picture, we propose a simple analytical approximation based on the analogy with standard capillary relaxation of elongated droplets. The model provides expressions for the relaxation and arrest times as a function of the diffusion coefficient of the gelling agent and the droplet viscosity. In particular, we show that it is the bending stiffness of the growing shell which slows down the relaxation and may leave it incomplete. The characteristic timescales for these phenomena are determined and discussed.

3 Materials and methods

The suspensions are mixtures of sodium alginate and zirconia particles. The sodium alginates are purchased from AGI with a molar mass of 250 kg/mol and a polydispersity index of 1.7. The zirconia particles, with a radius of 150 nm (dynamic light scattering) are obtained from Saint-Gobain Zirpro (HanDan, China). We use zirconia particles to obtain a better contrast for imaging and to increase the density of the droplets so that they sediment to the bottom of the liquid reservoir quickly after impacting the bath. In all the experiments described here the samples are composed of 8 vol % of zirconia and 0.8 vol % of alginate. The flow curve of the resulting suspension is shown in Section 1 of the SI. To produce the suspension droplets we use a 100 mL syringe equiped with a 400 µm diameter needle. Using a syringe-pump, we produce droplets of diameter 2.5 mm, which are dripped into a calcium bath (calcium chloride hexahydrate - Sigma-Aldrich) from heights ranging between 2 and 20 cm. The impact and relaxation of the droplets are monitored using a high-speed camera (Photron Fastcam mini) equiped with a 105 mm macro and a focal doubler from Sigma. A LED back light (50000 cd/m2 SLLUB White from Phlox) is placed behind the calcium bath.

For the numerical calculations, we use the finite element software Abaqus [22] with the implicit solver and a large strain formulation. The viscous newtonian material is modelled as viscoelastic (a one-term Prony series) with a negligible long time modulus. The calcium concentration is mapped to the temperature field. Williams Landel Ferry (WLF) scaling of the viscoelastic relaxation time is usually applied to model the glass transition in polymers:

here we use it (in reverse) to implement the Ca mediated solidification. Finally, the contraction of the solid is emulated by a negative thermal expansion. The exact implementation is detailed in Section 5 of the SI and example source files are included.

4 Results

4.1 Elongated droplets become spherical upon gelation

We drip millimetric droplets of suspensions of alginate and zirconia into an aqueous bath containing varying concentrations of calcium ions. The divalent calcium ions bind the anionic alginate chains together by electrostatic interactions leading to the formation of a hydrogel. Such type of alginate calcium system is widely used to produce gel beads for drug and cell encapsulation purposes [23, 24, 25] or water decontamination [26, 27]. Figure 1a presents high speed camera images of the evolution of the droplets while Figure 1c is a schematic drawing of the dripping process. As the droplets hit the surface of the bath, they elongate because their kinetic energy is converted into interfacial energy with the creation of droplet/air interface. The elongated droplets subsequently cross the interface and sink into the bath. The calcium ions diffuse into the alginate droplets and induce the gelation of the alginate: a gelled elastic layer forms at the interface between the droplet and the calcium bath and grows radially inwards.

Looking closely at the droplets reaching the bottom of the bath under schlieren observation conditions, we observe a bright aureola around the

gelling droplet (Figure 1b). It is due to the expulsion of water from the gelled layer. It is clearly visible because the expelled water is less salty than the surrounding calcium bath, with a lower refractive index, and rises to the top of the bath because of its lower density (1.1 g/cm^3 for the 158 g/L calcium bath versus 1 g/cm^3 for pure water).

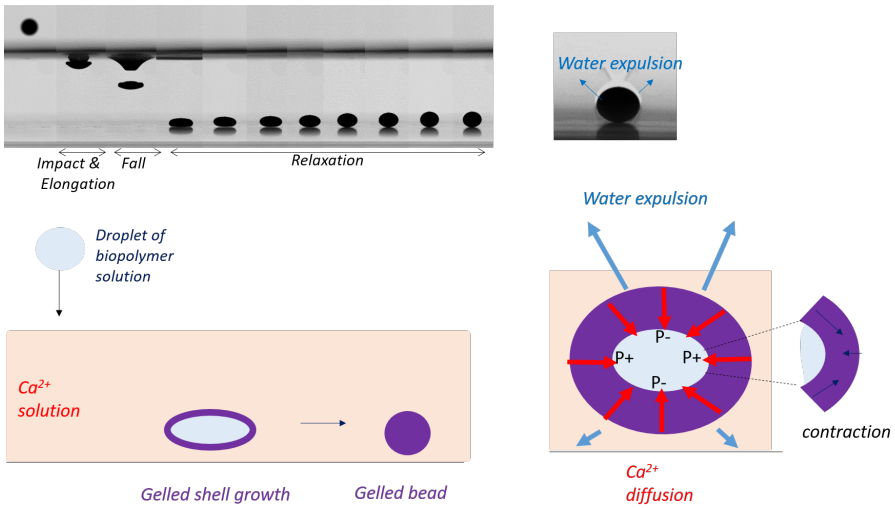

Figure 1: Alginate-zirconia droplets impacting and relaxing in a bath. a) high speed camera images of the dripping and gelling process and b) image of the droplet expelling pure water c) shematic drawing of the dripping and gelling process and d) diffusion of calcium into the droplets, water expelled from the gelling droplets and pressure difference between the highly curved apex and zones of lower curvature.

To determine how the calcium concentration affects the thickness evolution of the gelled layer we collect the droplets at various gelation times and calcium concentrations, cut them with a knife and measure the thickness of the gelled shell with a microscope (Figure 2 b). Fitting the data with a diffusion model in spherical geometry enables us to estimate the diffusion coefficient of the calcium ions, which is our fitting parameter. We find that it is of the order of $\kappa = 3 \times 10^{-10}$ m^2/s consistently with previous studies

[28, 29]. As expected for a diffusion controlled process the shell growth rate increases with calcium concentration. As an example the time needed to obtain gelation across the whole droplets decreases from 2000 to 500 seconds when the calcium concentration increases from 5 g/L to 158 g/L.

We follow the shape relaxation kinetics by measuring the aspect ratio of the gelling droplets: it is defined as the ratio of the longest to the smallest dimension. For a calcium concentration of 1.58 g/L the aspect ratio of the droplets barely decreases and the droplets remain strongly elongated with a final aspect ratio close to 3. For calcium concentrations between 5 and 158 g/L, the droplets relax toward spherical shapes with final aspect ratios closer to unity.

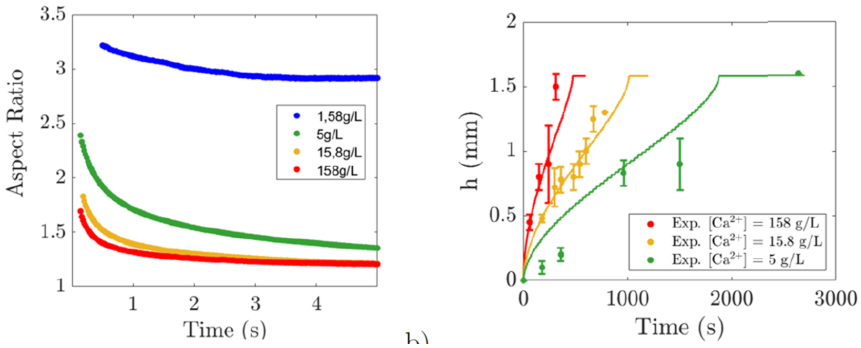

Figure 2: Influence of calcium concentration on the relaxation process and thickness growth of the gelled layer for an impact height of 10 cm. a) Evolution of the aspect ratio of the beads upon gelation for different calcium concentrations between 1.58 g/L and 158 g/L b) thickness of the gelled layer as a function of time for calcium concentrations 5 g/L, 15.8 g/L and 158 g/L- The continuous lines are obtained by fitting the data with a diffusion model in spherical coordinates with a diffusion coefficient $\kappa = 3 \times 10^{-10}$ m^2/s

The results presented so far show that the relaxation kinetics and the growth of the gelled layer are influenced by calcium concentration. The relaxation process of the droplets is therefore correlated with the existence

of a gelation reaction at the interface between the droplet and the aqueous bath, which leads to the expulsion of water from the gelling membrane. These observations can be rationalized as shown in Figure 1 d. As calcium diffuses into the droplet, an elastic membrane forms at the droplet surface and grows inwards. Syneresis drives the expulsion of water from the membrane and results in a volume contraction of the gelled membrane. The gelled membrane can contract freely in the direction normal to the surface but contraction is constrained in the direction parallel to the surface because the ungelled liquid core is incompressible. This constrained contraction results in tensile stresses within the gelled layer, which acts as a membrane and drives the relaxation of the droplet. We note that the difference of osmotic pressure between the droplet and the calcium bath may also induce an outward flow from the droplet toward the bath through the gelling membrane. However this flow causes a volume reduction of the liquid core and hence a compressive stress inside the membrane that cannot account for the relaxation of the gelling droplets. We therefore emphasize that it is the volume contraction of the thin gelling membrane that causes a tensile stress in the membrane and the subsequent relaxation of the beads toward more spherical shapes.

4.2 Numerical simulation of the relaxation of gelling droplets

To confirm qualitatively the mechanism proposed above, we have also carried out numerical simulations including a minimal number of ingredients. We present below the three key ingredients that enable to reproduce the exper-

imental observations. Simulating droplets, which undergo a liquid-to-solid transition is a difficult task as most numerical methods available are either adapted to describe the relaxation of liquids droplets [30, 31, 32] or the deformation of solids *e*.g. with surface tension [33, 34, 35] but not the transformation from liquid-to-solid. For the numerical calculations, we use finite element modeling (FEM) within a lagrangian description in which elasticity and free surfaces are readily included. The three main elements that we take into account are the following i. the diffusion of the calcium ions into the droplets ii. the resulting material tranformation from liquid to solid iii. the simultaneous contraction of the solid layer. We describe qualitatively below the method we use to include these three ingredients (more technical details can be found in Section 5 of the SI) and then analyze the relaxation as a function of calcium concentration and initial aspect ratio of the droplets.

Diffusion of the calcium ions into the droplets. At the surface of the elongated droplet we keep the calcium concentration $\mathcal{C}$ constant equal to the concentration of the bath $\mathcal{C}_{bath}$ while inside the droplet, $\mathcal{C}$ is initially zero and then increases over time with a Fickian law. The diffusion coefficient (typically $\kappa = 0.001$) is chosen such that the diffusion time scale is long compared to the relaxation time of the liquid.

Transformation of the liquid core into a solid. For the sake of simplicity we choose to neglect the complex rheological properties of the liquid core. We model it as a linear viscoelastic solid with a negligible long time elastic modulus μ_∞ and a relaxation time $\tau = \eta/\mu_0$ where η is the viscosity and μ_0 the short time elastic modulus. To simulate the gelation process induced by the calcium we impose a sharp increase of the relaxation time with the

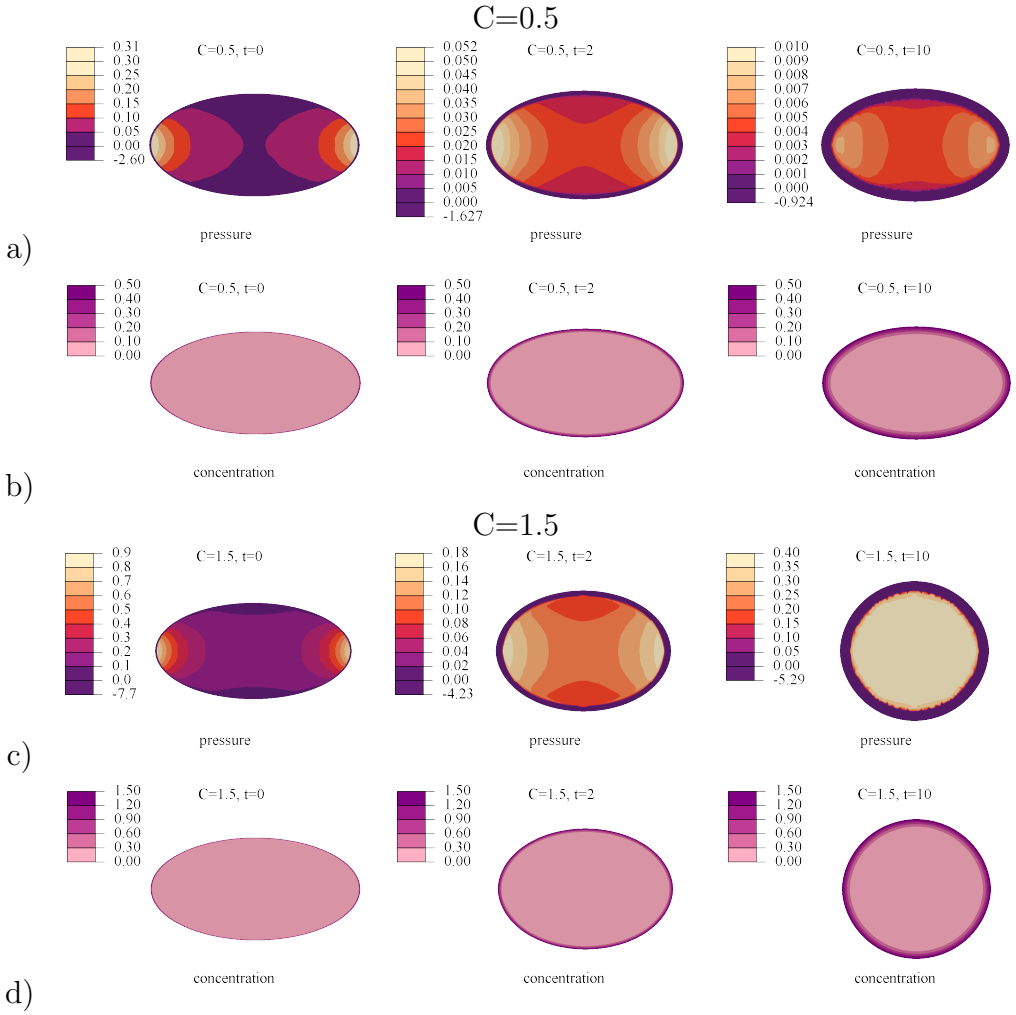

Figure 3: Representative snapshots of the simulation results for the relaxation of gelling droplets for two calcium concentrations. a) pressure distribution for three successive times for $C = 0,5 < \mathcal{C}_{sat}$ - b) calcium concentration distribution for $\mathcal{C} = 0.5$ - c) pressure distribution for a calcium concentration $C = 1,5 > \mathcal{C}_{sat}$ - d) calcium concentration distribution for C=1.5

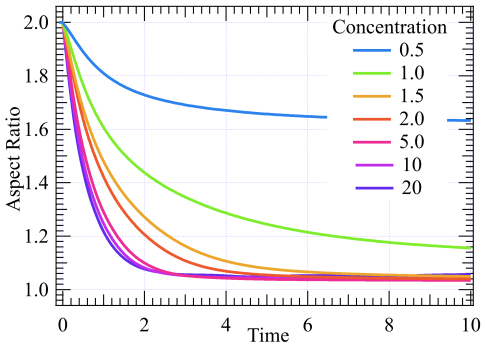

Figure 4: Relaxation of a gelling droplet: impact of the bath concentration on relaxation (initial aspect ratio 2 - standard values of the numerical parameters). The relaxation is much more efficient when the bath concentration exceeds the material saturation concentration $\mathcal{C}_{sat} = 1$. When the bath concentration is lower, the relaxation stalls.

calcium concentration $\mathcal{C}$, while keeping the short time elastic modulus μ_0 constant. In the regions where the calcium diffuses, the material relaxation time becomes much larger than the typical diffusion time, *i.e.* the liquid effectively turns into an elastic solid with a an elastic modulus given by the short time modulus μ_0.

Contraction of the elastic layer due to syneresis. Finally, the material's contraction under the action of calcium is accounted for by applying an isotropic material strain $\epsilon_{\mathcal{C}}$ proportional to the calcium concentration. We take

$$\epsilon_{\mathcal{C}} = \alpha\, \mathcal{C} \quad \text{for} \quad \mathcal{C} < \mathcal{C}_{sat} \quad \text{or} \quad \epsilon_{\mathcal{C}} = \alpha\, \mathcal{C}_{sat} \quad \text{for} \quad \mathcal{C} \geq \mathcal{C}_{sat} \tag{1}$$

In Equation 1, we have introduced a saturation concentration $\mathcal{C}_{sat}$ above which no more contraction is incurred. We have found that this threshold concentration $\mathcal{C}_{sat}$ is a necessary ingredient that enables to reproduce the experimental observations. The physical meaning of $\mathcal{C}_{sat}$ will be discussed

later. In the following we use this saturation concentration to normalize the concentrations ($\mathcal{C}_{sat} = 1$). Furthermore we set the contraction $\alpha = -0.1$ which is qualitatively consistent with the macroscopic volume loss $\delta V/V_0 \approx 15\%$ measured at long times (see Section 3 of the SI). One expects $\delta V/V_0 = 3\alpha$.

Because the physics is similar but the model is simpler, the calculations are performed in plain strain. The standard initial geometry is an ellipse with radii $R_X = \sqrt{3}$ and $R_Y = 1/\sqrt{3}$ *i.e.* an aspect ratio $AR = 3$. We calculate the evolution of the droplet shape as well as the pressure fields and distribution of calcium concentration. Full relaxation would result in a circle of radius $R = 1$. We first consider the influence of the calcium concentration in the bath, then the influence of different initial aspect ratios.

In Figures 3a and 3b we show distributions of pressure and calcium concentration at different times for calcium bath concentrations $\mathcal{C}_{bath}$=0.5 and $\mathcal{C}_{bath}$=1.5 ie below and above $\mathcal{C}_{sat}$. For both cases we observe a relaxation process where the aspect ratio decreases. The relaxation is faster and more complete for $\mathcal{C}_{bath}$=1.5 than for $\mathcal{C}_{bath}$=0.5. Turning to the pressure field, we find that the highest pressures are located at the apex of the ellipsoids, where the curvature is the highest. The pressure gradient between areas of high and low curvature induces a flow inside the liquid core from the apexes towards the center of the drop, leading to the shape relaxation toward a lower aspect ratio. This pressure field is very similar to the one expected in the case of the capillary relaxation an elongated droplet of Newtonian fluid in an immiscible and non gelling liquid whose simulation results are provided in Section 5.3 of the SI. We note that the experimental result obtained for a droplet

of suspension impacting a non gelling bath containing an immiscible organic oil is presented in Section 4 of the SI. While for capillary relaxation it is the interfacial tension, which drives the relaxation process, in our gelling droplets it is the contraction of the gelled membrane, which induces a tensile stress parallel to the surface of the droplet. Thus, at the early stages of calcium diffusion, the gelled layer forms an elastic and contracting membrane around the incompressible viscous core (Fig. 1 d). The tensile stress in this membrane acts as an effective interfacial tension, generating a pressure gradient and a flow.

Fig. 4 presents the evolution of the aspect ratio for several $\mathcal{C}_{bath}$ values. Clearly the main experimental trends obtained in Fig. 2 a are accounted for by the numerical model. Indeed in both experiments and simulations the relaxation leads to lower final aspect ratios when the calcium concentration increases. When $\mathcal{C}_{bath}$ is below the threshold $\mathcal{C}_{sat}$, relaxation stops while the droplet is still elongated (Fig. 3a and Fig. 4). In the experiments a critical calcium concentration is also found (Fig. 2). Indeed below 5 gl^{-1} the droplets relaxation is largely incomplete and the aspect ratio remains of the order of three over the whole experiment while above 5 gl^{-1} the droplets relax toward spherical shapes and aspect ratios close to 1. We note that this critical calcium concentration of 5 gl^{-1} corresponds to 0.05 M, half the concentration of the carboxylic acid groups of the alginate (0.1 M). We suggest that this critical calcium concentration corresponds to the concentration required for a saturation of the carboxylic groups by the calcium ions and hence a saturation of the cross-linking process and contraction.

To further check the relevance of our numerical model, we consider exper-

imental results for different initial aspect ratios. The initial aspect ratio of the droplet is varied between 1.3 and 3 by changing the dripping height. The data (Fig. 5 a) show that the initial aspect ratio plays a significant role on the final droplet shape: with a lower initial aspect ratio, the droplet reaches full relaxation, while more elongated droplets do not evolve beyond a partially relaxed state.

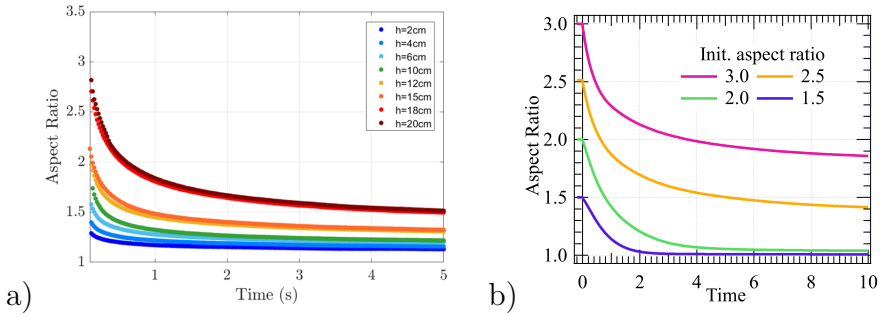

Figure 5: Shape evolution with different initial aspect ratios a) experimental results for a calcium concentration of 158 g/L b) numerical simulations for different initial aspect ratios, from 1.5 to 3. The effect of the initial aspect ratio is clearly non linear.

Numerical simulations are carried out with a similar range of initial aspect ratios. They reproduce the major features of the measurements very well (Fig. 5 b): similar relaxation times are found for all the investigated cases. However the final shapes are more elongated when the initial aspect ratio increases. To explain this effect of initial elongation, we note that the pressure gradient is mainly localized near the apexes (Fig. 3) and the flow is mostly located in these high curvature areas. For more elongated droplets, the flow does not reach the central part of the droplets and the relaxation is much less effective. This is clearly a non linear effect due to geometry, and is quite similar to the end-pinching effect in the relaxation of liquid droplets [36].

5 Mechanisms driving and arresting the droplet shape evolution

5.1 Syneresis as a driving force for relaxation

For more insight into the relaxation process, its driving force and its limiting mechanism, we have developed a simple model based on scaling arguments. As shown by the numerical simulations, a growing surface layer solidifies and contracts. The ensuing tensile stresses induce pressure gradients, which drive a viscous flow and the relaxation of the gelling droplet. This process presents some similarity with the capillary relaxation of elongated liquid droplets under the action of interfacial energy γ (Laplace pressure) [32]. Considering the spherical surface of a liquid droplet of radius R (Fig. 1 a) and applying a first order perturbation of amplitude u, the evolution equation reads :

$$\eta \frac{du}{Rdt} \simeq -\gamma \frac{u}{R^2} \tag{2}$$

where the left hand side is the viscous stress and the right hand side is the Laplace pressure gradient [30, 31]. We directly obtain an exponential relaxation with the usual characteristic time $t_r \simeq \eta R/\gamma$ (see Section 5.3 of the SI).

For the solidifying droplet, we use the same framework replacing the interfacial energy γ by the membrane tensile stresses resulting from the syneresis

$$\gamma(t) \simeq \mu_0 \epsilon h(t) \tag{3}$$

The biaxial in-plane stress generated by the layer contraction is of order $\mu_0\epsilon$ and is integrated over the gelled layer thickness $h(t)$. This thickness is controlled by the calcium diffusion so that

$$h(t) \simeq \sqrt{\kappa t} \tag{4}$$

Combining Equations 2, 3 and 4 yields

$$\frac{du}{d\ (t/t_c)^{3/2}} \simeq -u \tag{5}$$

Solutions are compressed exponentials with an exponent 3/2

$$u(t) \propto \exp(-(t/t_c)^{\frac{3}{2}}) \tag{6}$$

with the characteristic time

$$t_c = \left(\frac{\eta R}{3\mu_0\epsilon\sqrt{\kappa}}\right)^{\frac{2}{3}} \tag{7}$$

This relaxation time rewrites

$$t_c = \left(\frac{\tau R}{3\epsilon\sqrt{\kappa}}\right)^{\frac{2}{3}} \tag{8}$$

With our standard parameter values $\tau \simeq 0.01$, $R \simeq 1$, $\epsilon \simeq 0.1$ and $\kappa \simeq 0.001$, we find that t_c is of the order of unity as expected. Moreover, when plotted as a function of t_c (Fig. 6), the numerical results calculated for various values of τ collapse, confirming the simple scaling relations Eqs. 6 and 7 in the first

stage of the relaxation.

Turning now to the experimental data, the rheology of the suspension is complex, but a reasonable value for the viscosity is $\eta \simeq$ 1 Pa.s (see Sections 1 and 4 of the SI that takes into account the viscosity of the suspension at the impact shear rate $\dot{\gamma} \approx U/D \approx 100$ s-1, with $U \approx 1$ m/s the impact velocity and $D \approx 1$ mm the diameter of the drop). Using a Young's modulus $3\mu_0$ of approximately 10 kPa (see Section 2 of the SI), $\kappa \simeq 3 \times 10^{-10}$ m^{2}s^{-1}, $R_0 = 1 \times 10^{-3}$m, we obtain a rough estimate $t_c \simeq 0.2$ s, which is consistent with the data (Fig. 2 a).

Expressions Eqs. 7 or 8 for the characteristic time of the droplet relaxation highlight the competition between the build-up of surface stress through diffusion, solidification and contraction and the viscous resistance due to the flow. This simple description matches the data in the early stages of relaxation. However, Eq. 6 predicts that an elongated droplet should always relax towards a sphere which is not what we observe in our experiments and simulations.

5.2 Arresting mechanism for the relaxation

To identify the relaxation limiting mechanism, we note that the driving force, the surface stress, results from the combination of contraction and elasticity of the gelled layer. However, the formation of an elastic shell around the drops also implies an increasing bending stiffness which resists further deformation as the surface layer is gradually turning from a thin membrane to a shell. The bending stiffness scales as $3\mu_0 h^3$ so that the bending energy per unit

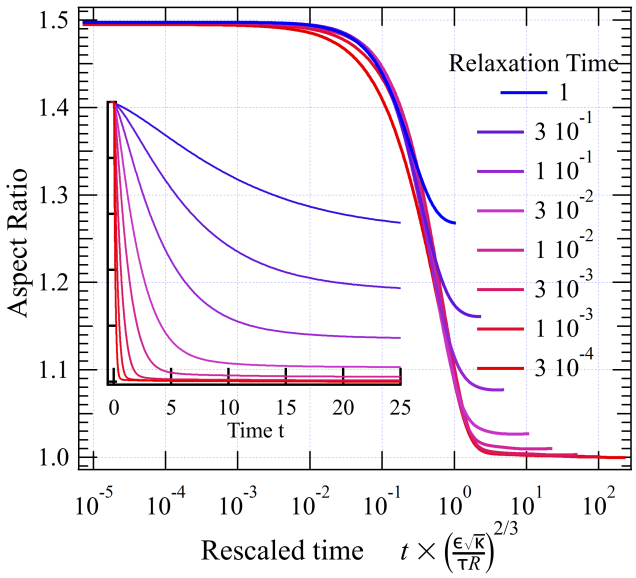

Figure 6: Simulated shape evolution for different material relaxation times τ for an initial aspect ratio 1.5 (insert). The relaxation curves collapse when time is rescaled according to Eq. 7 except for the final stage.

area, evaluated from the curvature variation u/R^2 of the gelled layer, scales as $\mathcal{E}_{bend} \approx 3\mu_0 h^3 (\frac{u}{R^2})^2$ and the pressure required for a variation u of the curvature radius is

$$P_{bend} \approx 3\mu_0 \left(\frac{h}{R}\right)^3 \frac{u}{R} \tag{9}$$

With this additional mechanism, the equation of evolution now reads

$$\eta \frac{du}{Rdt} \simeq 3\mu_0 \left(-\epsilon \frac{\sqrt{\kappa t}}{R^2} + \frac{(\kappa t)^{3/2}}{R^4}\right) u \tag{10}$$

This relation shows that bending stiffness tends to counteract the effective surface tension and that they balance each other for a characteristic time

$$t_s \simeq \frac{R^2 \epsilon}{\kappa} \tag{11}$$

at which the relaxation arrests. Therefore, the condition for complete relaxation is $t_s \gg t_c$. For example, complete relaxation ensues when the material contraction exceeds a threshold strain ϵ_t given by

$$\epsilon_t = \left(\frac{\sqrt{\tau\kappa}}{R} \right)^{\frac{4}{5}} \tag{12}$$

This expression highlights the equivalent roles played by the material relaxation time and the diffusion coefficient : while a smaller relaxation time speeds up the viscous flow, a smaller diffusion coefficient delays the thickening process of the layer, giving more time for relaxation. With our standard parameter values $R = 1$ and $\kappa = 0.001$, and with $\tau = 0.01$ which is seen to be the crossover value between the full and the partial relaxation regimes in fig. 6), we find $\epsilon_t = 0.01$ which is indeed small compared to our reference material contraction $\epsilon = 0.1$.

Our results also enable to understand the existance of a threshold calcium concentration necessary for complete relaxation (Figs 2 a). Below the saturation value, the contraction ϵ grows with calcium concentration so the lowest calcium concentrations fail to meet the requirement (Eq. 12) for full relaxation.

This simple model captures the incomplete relaxation found in both experiments and simulations. It is important to note that the transformation of the surface layer into a solid drives two opposite mechanisms. While solidification and contraction induce tensile stresses in the gelled layer which initially act as a tensile membrane driving the relaxation, the same transformation also sets up a bending moment which increasingly resists the defor-

mation of the gelled shell eventually leading to the arrest of the relaxation process.

At this stage, we find it interesting to compare non equilibrium gelling droplets to more complex non equilibrium systems such as living cells where the contraction of the actomyosin cortex controls tensile stresses and hence the morphogenesis of living cells and tissues [37, 38, 39, 40]. In particular one of the virtues of this active process is to maintain the thickness of the cortex constant while developping tension, thus avoiding the deformation limiting bending stiffness. Because of this dynamic reorganisation, the cortex can act dynamically like the surface tension of a simple liquid.

6 Conclusion

We have studied the shape evolution of solidifying droplets during gelation. After initial elongation, the cross-linking agent, calcium ions, diffuses into the droplets resulting in the inward growth of a gelling layer. Combining experimental observations and numerical simulations we showed that the resulting volume contraction and developping elasticity of the gelling layer result in tensile stresses which induce pressure gradients between the areas of high and low curvatures trigering a flow of ungelled liquid inside the droplet and relaxion towards a spherical shape. By analogy with the capillary relaxation of viscous elongated droplets under the action of surface tension, we have developped an simple analytical model based on the balance between the mechanical stress in this tensile membrane and the viscous stress in the liquid core. With this model we are able to express the characteristic time of

the relaxation as a function of the calcium diffusion coefficient, the viscosity of the liquid core and the droplet radius. The tensile stress grows over time as the membrane thickness increases, however bending stiffness of the shell resisting the change of shape also increases over time. The resulting resistance to curvature variations may eventually balance the tensile stress and result in an incomplete relaxation. We have proposed a criterion to determine the parameter region where this does not occur and full relaxation is attained. These results help in understanding the complex phenomenology of the deformation of non-equilibrium bodies undergoing phase transformation.

7 Acknowledgements and funding

We acknowledge R. Valette, N. Bremond, L. Ramos and A. Pereira for stimulating discussions as well as Saint-Gobain for funding.

8 Conflict of interest

The authors have no conflict of interest to declare.

References

[1] Claas Willem Visser, Tom Kamperman, Lisanne P Karbaat, Detlef Lohse, and Marcel Karperien. In-air microfluidics enables rapid fabrication of emulsions, suspensions, and 3d modular (bio) materials. *Science advances*, 4(1):eaao1175, 2018.

[2] Michaela Klotz, Idris Amirouche, Christian Guizard, Céline Viazzi, and Sylvain Deville. Ice templating—an alternative technology to produce micromonoliths. *Advanced Engineering Materials*, 14(12):1123–1127, 2012.

[3] Jos De Jong, Hans Reinten, Herman Wijshoff, Marc Van Den Berg, Koos Delescen, Rini Van Dongen, Frieder Mugele, Michel Versluis, and Detlef Lohse. Marangoni flow on an inkjet nozzle plate. *Applied physics letters*, 91(20):204102, 2007.

[4] Sidhanth Tyagi, Cécile Monteux, and Sylvain Deville. Solute effects on the dynamics and deformation of emulsion droplets during freezing. *Soft Matter*, 18(21):4178–4188, 2022.

[5] Robin BJ Koldeweij, Pallav Kant, Kirsten Harth, Rielle de Ruiter, Hanneke Gelderblom, Jacco H Snoeijer, Detlef Lohse, and Michiel AJ van Limbeek. Initial solidification dynamics of spreading droplets. *Physical review fluids*, 6(12):L121601, 2021.

[6] François Boulogne and Anniina Salonen. Drop freezing: fine detection of contaminants by measuring the tip angle. *Applied Physics Letters*, 116(10):103701, 2020.

[7] Rodolphe Grivet, Antoine Monier, Axel Huerre, Christophe Josserand, and Thomas Séon. Contact line catch up by growing ice crystals. *Physical Review Letters*, 128(25):254501, 2022.

[8] Detlef Lohse and Xuehua Zhang. Physicochemical hydrodynamics of droplets out of equilibrium. *Nature Reviews Physics*, 2(8):426–443, 2020.

[9] E Pezron, L Leibler, A Ricard, and R Audebert. Reversible gel formation induced by ion complexation. 2. phase diagrams. *Macromolecules*, 21(4):1126–1131, 1988.

[10] Kurt Ingar Draget, Olav Gåserød, Ingrid Aune, Peder O Andersen, Bente Storbakken, Bjørn Torger Stokke, and Olav Smidsrød. Effects of molecular weight and elastic segment flexibility on syneresis in ca-alginate gels. *Food Hydrocolloids*, 15(4-6):485–490, 2001.

[11] Thibaut Divoux, Bosi Mao, and Patrick Snabre. Syneresis and delayed detachment in agar plates. *Soft Matter*, 11(18):3677–3685, 2015.

[12] Bosi Mao, Thibaut Divoux, and Patrick Snabre. Normal force controlled rheology applied to agar gelation. *Journal of Rheology*, 60(3):473–489, 2016.

[13] Dinesh Chandra and Alfred J Crosby. Self-wrinkling of uv-cured polymer films. *Advanced Materials*, 23(30):3441–3445, 2011.

[14] Thierry Mora and Arezki Boudaoud. Buckling of swelling gels. *The European Physical Journal E*, 20(2):119–124, 2006.

[15] Anna Lee, Dong Yan, Matteo Pezzulla, Douglas P Holmes, and Pedro M Reis. Evolution of critical buckling conditions in imperfect bilayer shells through residual swelling. *Soft Matter*, 15(30):6134–6144, 2019.

[16] Jia Liu, Tianyu Gu, Sicong Shan, Sung H Kang, James C Weaver, and Katia Bertoldi. Harnessing buckling to design architected materials that

exhibit effective negative swelling. *Advanced Materials*, 28(31):6619–6624, 2016.

[17] J William Boley, Wim M Van Rees, Charles Lissandrello, Mark N Horenstein, Ryan L Truby, Arda Kotikian, Jennifer A Lewis, and L Mahadevan. Shape-shifting structured lattices via multimaterial 4d printing. *Proceedings of the National Academy of Sciences*, 116(42):20856–20862, 2019.

[18] Jungwook Kim, James A Hanna, Myunghwan Byun, Christian D Santangelo, and Ryan C Hayward. Designing responsive buckled surfaces by halftone gel lithography. *science*, 335(6073):1201–1205, 2012.

[19] Douglas P Holmes. Elasticity and stability of shape-shifting structures. *Current opinion in colloid & interface science*, 40:118–137, 2019.

[20] Verónica Trujillo, Jungwook Kim, and Ryan C Hayward. Creasing instability of surface-attached hydrogels. *Soft Matter*, 4(3):564–569, 2008.

[21] Changjin Huang, Zilu Wang, David Quinn, Subra Suresh, and K Jimmy Hsia. Differential growth and shape formation in plant organs. *Proceedings of the National Academy of Sciences*, 115(49):12359–12364, 2018.

[22] *Abaqus reference manual*. HKS, Providence, 2016.

[23] Wayne R Gombotz and SiowFong Wee. Protein release from alginate matrices. *Advanced drug delivery reviews*, 31(3):267–285, 1998.

[24] Joseph AM Steele, J-P Hallé, D Poncelet, and RJ Neufeld. Therapeutic

cell encapsulation techniques and applications in diabetes. *Advanced drug delivery reviews*, 67:74–83, 2014.

[25] Hanne Hjorth Tønnesen and Jan Karlsen. Alginate in drug delivery systems. *Drug development and industrial pharmacy*, 28(6):621–630, 2002.

[26] Sakshi Thakur. An overview on alginate based bio-composite materials for wastewater remedial. *Materials Today: Proceedings*, 37:3305–3309, 2021.

[27] Mahmoud Nasrollahzadeh, Mohaddeseh Sajjadi, Siavash Iravani, and Rajender S Varma. Starch, cellulose, pectin, gum, alginate, chitin and chitosan derived (nano) materials for sustainable water treatment: A review. *Carbohydrate polymers*, 251:116986, 2021.

[28] Etude de la formation de fibres en microfluidique : compétition entre mise en forme et gélification de fluides complexes sous écoulement, 2011.

[29] Hae-Sung Kim. A kinetic study on calcium alginate bead formation. *Korean Journal of Chemical Engineering*, 7(1):1–6, 1990.

[30] H A Stone. Dynamics of drop deformation and breakup in viscous fluids. *Annual Review of Fluid Mechanics*, 26(1):65–102, 1994.

[31] K Moran, A Yeung, and J Masliyah. Shape relaxation of an elongated viscous drop. *Journal of colloid and interface science*, 267(2):483–493, 2003.

[32] Dominique Barthès-Biesel. Capsule motion in flow: Deformation and membrane buckling. *Comptes Rendus Physique*, 2009.

[33] Dadhichi Paretkar, Xuejuan Xu, Chung-Yuen Hui, and Anand Jagota. Flattening of a patterned compliant solid by surface stress. *Soft matter*, 10(23):4084–4090, 2014.

[34] Serge Mora, Corrado Maurini, Ty Phou, Jean-Marc Fromental, Basile Audoly, and Yves Pomeau. Solid drops: Large capillary deformations of immersed elastic rods. *Physical review letters*, 111(11):114301, 2013.

[35] J Dollhofer, A Chiche, V Muralidharan, C Creton, and CY Hui. Surface energy effects for cavity growth and nucleation in an incompressible neo-hookean material—-modeling and experiment. *International Journal of Solids and Structures*, 41(22-23):6111–6127, 2004.

[36] Howard A Stone and L Gary Leal. Relaxation and breakup of an initially extended drop in an otherwise quiescent fluid. *Journal of Fluid Mechanics*, 198:399–427, 1989.

[37] Jean-Yves Tinevez, Ulrike Schulze, Guillaume Salbreux, Julia Roensch, Jean-François Joanny, and Ewa Paluch. Role of cortical tension in bleb growth. *Proceedings of the National Academy of Sciences*, 106(44):18581–18586, 2009.

[38] Martin P Stewart, Jonne Helenius, Yusuke Toyoda, Subramanian P Ramanathan, Daniel J Muller, and Anthony A Hyman. Hydrostatic pressure and the actomyosin cortex drive mitotic cell rounding. *Nature*, 469(7329):226–230, 2011.

[39] Daniel A Fletcher and R Dyche Mullins. Cell mechanics and the cytoskeleton. *Nature*, 463(7280):485–492, 2010.

[40] Thomas Pujol, Olivia du Roure, Marc Fermigier, and Julien Heuvingh. Impact of branching on the elasticity of actin networks. *Proceedings of the National Academy of Sciences*, 109(26):10364–10369, 2012.